ISSN 0915-633X

NATIONAL INSTITUTE FOR FUSION SCIENCE

Stochasticity in the Josephson Map

Y. Nomura, Y.H. Ichikawa and A.T. Filippov

(Received - Apr. 10, 1996)

NIFS-413 Apr. 1996

RESEARCH REPORT
NIFS Series

NAGOYA, JAPAN

Stochasticity in the Josephson Map

[1] *Y.Nomura* , [2] *Y.H.Ichikawa*

and

[3] *A.T.Filippov*

[1] *Fukui National College of Technology, Sabae, 916, Japan*

[2] *College of Engineering, Chubu University, Kasugai,487,Japan*

[3] *Joint Institute for Nuclear Research, Dubna, 141980, Russian Federation*

Abstract

The Josephson map describes nonlinear dynamics of systems characterized by standard map with the uniform external bias superposed. The intricate structures of the phase space portrait of the Josephson map are examined on the basis of the tangent map associated with the Josephson map. Numerical observation of the stochastic diffusion in the Josephson map is examined in comparison with the renormalized diffusion coefficient calculated by the method of characteristic function. The global stochasticity of the Josephson map occurs at the values of far smaller stochastic parameter than the case of the standard map.

Keywords

Josephson map, Standard map, Symmetry breaking

[1] E-mail: nomura@fingw1.ip.fukui-nct.ac.jp
[2] E-mail: ichikawa@ms.nfs.ac.jp
[3] E-mail: FILIPPOV@THEOR.JINRC.DUBNA.SU

1 Introduction

Dynamics of fluxons in long Josephson junctions has attracted deep interests inspired with the physical principle and possible applications[1][2]. Referring to the real systems, we observe that effect of spatial inhomogeneities is one of the central issues of properties of long Josephson junctions. One of the present authors (A.T.F) has worked intensively on formation of stable bound states of fluxons in the inhomogeneous long Josephson junctions[3]~[6]. The predicted bound fluxons have been observed experimentally [7].

One of the present authors (A.T.F) in collaboration with Gal'pern[8] examined bound states, bifurcation and static chaos in Josephson lattice in detail. The static magnetic flux distribution $\phi(x)$ in a homogeneous lattice may be described by the equation

$$\frac{d^2}{dx^2}\phi(x) = \sum_n \mu\delta(x - x_n)\sin\phi(x) + \gamma. \tag{1}$$

Then, the flux distribution at the $n-th$ interval $x_n < x < x_{n+1}$ is expressed as

$$\phi_n(x) = a_n + b_n(x - x_n) + \frac{1}{2}\gamma(x - x_n)^2, \tag{2}$$

Assuming the lattice to be periodic ($x_{n+1} - x_n = \Delta$), we can determine the coefficients a_n and b_n by solving the equation

$$\begin{aligned} a_n &= a_{n-1} + \bar{b}_{n-1} + \frac{1}{2}\bar{\gamma}, \\ \bar{b}_n &= \bar{b}_{n-1} + \bar{\mu}\sin a_n + \bar{\gamma} \end{aligned} \tag{3}$$

with the abbreviations $\bar{b}_n = b_n\Delta$, $\bar{\mu} = \mu\Delta$ and $\bar{\gamma} = \gamma\Delta^2$. Setting $a_n = 2\pi X_n$, $\bar{b}_n + \frac{1}{2}\bar{\gamma} = 2\pi P_{n+1}$, we can reduce Eq.(3) to the following set of recurrence equations

$$\begin{aligned} X_{n+1} &= X_n + P_{n+1} \\ P_{n+1} &= P_n - \frac{K}{2\pi}\sin(2\pi X_n) + \Gamma \end{aligned} \tag{4}$$

where $K = -\bar{\mu}$ and $\Gamma = \bar{\gamma}/2\pi$. In the original problem of the Josephson lattice, Eq.(4) poses the boundary value problem for the total length of lattice size L. While we may impose the periodic boundary condition with modules 1 on Eq.(4). We may call Eq.(4) with the boundary condition of modules 1 the Josephson map. The Josephson map Eq.(4) attracts our special interests, since the bias Γ gives rise to the symmetry breaking for the standard map. Within the context of nonlinear dynamics,

the Josephson map stands for physical phenomena for the systems described by the standard map with uniform external field super imposed.

In the second section, we present general feature of the stochasticity of the Josephson map. We will analyze the observed phase space characteristics in terms of the basic properties of the Josephson map in the third section. In the fourth section, we discuss preliminary analysis of the stochastic properties of the Josephson map by investigating the diffusion process.

2 Phase-space Portrait of the Josephson map

In order to grasp the effect of symmetry breaking for the standard map and to understand the characteristic features of the Josephson map, we show the phase-space portrait of the Josephson map for the various values of the stochastic parameter K and the bias parameter Γ in Fig.1.a) to 1.c). We notice that the Josephson map is invariant under the transformation of $X \to -X$, $P \to -P$, $\Gamma \to -\Gamma$ and $\Gamma \to 1-\Gamma$ with modules 1. So, it is enough to examine the range of $0 < \Gamma < +0.5$ for various values of the stochasticity parameter A. Throughout the present paper, the phase-space portraits of the mapping extend over the range of $-0.5 < P < +0.5$ in the ordinate and $-0.5 < X < +0.5$ in the abscissa.

Let us begin with the value of $K = 1.3$ as shown in Fig.1.a). For $\Gamma = 0$, the Poincaré-Birkhoff period-q bifurcation condition for the standard map

$$K(p/q) = 2\{1 - \cos(2\pi p/q)\} \tag{5}$$

confirms that the period-6 islands, but not the period-5 islands, born at the stable fixed point $(X = 0, P = 0)$[9]. Increasing the bias parameter Γ through 0.05 to 0.10, we see the central island shifts to the positive X-direction with compression in its size. At $\Gamma = 0.10$, we observe the interchange of stable points and unstable points of the period-6 islands. At $\Gamma = 0.15$, there appear ten white empty islands in the chaotic sea. At $\Gamma = 0.25$, the central island is washed out, while there appear three coherent structures. Increasing Γ to 0.40, we observe very dominant coherent structure, presumably the period-2 islands.

In Fig.1.b), we illustrate the similar fate of the phase-space portrait for the stochasticity parameter $K = 2.1$, for which we have the period-4 Poincaré-Birkhoff

islands at the center.(Eq.(5) gives $K(1/4) = 2.0$.) Increasing the bias parameter Γ through 0.15 to 0.20, we notice that the period-4 Poincaré-Birkhoff island at the center turns into the period-5 island, while four white island structure appears in the chaotic sea. Further increase of the bias parameter Γ leads to the period-2 structure as anticipated in Fig.1.a).

Fig.1.c) stands for the case of the stochastic parameter $K = 3.3$. The standard map with $\Gamma = 0$ accompanies two sets of the period-3 Poincaré-Birkhoff island, which appears like the period-6 island at the fringe of the islands. Because of the symmetry breaking with $\Gamma = 0.05$, one of the period-3 island survives with the interchange of the stability along the $P = 0$ axis. Now, increasing the bias parameter Γ through 0.10 to 0.3, we observe the typical period-3 squeezing process. At $\Gamma = 0.40$, we see the period-4 Poincaré-Birkhoff island at the center with some coherent structures in the chaotic sea. At $\Gamma = 0.45$, these coherent structure manifest themselves as if they are period-3 island. Lastly, at the value of $\Gamma = 0.50$, we observe the stable island structure at the position $(X \approx -0.25, P = 0)$ together with the original central island shifted to the position $(X \approx +0.25, P = 0)$, which is originated from the recovery of symmetry at $\Gamma = 0.5$.

We conclude the present section emphasizing that dynamical behavior predicted by the Josephson map exhibits a very intricate structure with sensitive dependence on the bias parameter Γ.

3 General Properties of the Josephson Map

Here, we will analyze the observed rich variation of the dynamics associated with the Josephson map.

Firstly, we notice the stationary points of the Josephson map (X_s, P_s) are determined from Eq.(4) as

$$\begin{aligned} X_s &= \frac{1}{2\pi}\sin^{-1}\{\frac{2\pi}{K}(\Gamma - l)\} \\ P_s &= m \end{aligned} \tag{6}$$

where l and m are integers. The values of $l = 0$ and $m = 0$ give the coordinate of

the fixed point as

$$\begin{aligned} X_f &= \frac{1}{2\pi}\sin^{-1}\left(\frac{2\pi\Gamma}{K}\right) \\ P_f &= 0 \end{aligned} \tag{7}$$

which confirms the observed shift of the central island upon the increase in the bias parameter Γ in Figs.1.a), b) and c). For the nonvanishing integer l, Eq.(6) gives the accelerator mode with the step size l. It is worth to notice that Eq.(4) does not admit the fixed points for both Γ and K small and for $\Gamma > K/2\pi$.

Now, the linear stability of these stationary points is determined from the tangent map of Eq.(4),

$$\begin{pmatrix} \Delta X_{n+1} \\ \Delta P_{n+1} \end{pmatrix} = \Delta T \begin{pmatrix} X_n \\ P_n \end{pmatrix} \equiv \begin{pmatrix} 1 - K\cos(2\pi X_s) & 1 \\ -K\cos(2\pi X_s) & 1 \end{pmatrix} \begin{pmatrix} \Delta X_n \\ \Delta P_n \end{pmatrix}. \tag{8}$$

The stability of the stationary point (X_s, P_s) is given in terms of the residue R as

$$0 < R \equiv \left(\frac{1}{2} - \frac{1}{4}tr(\Delta T)\right) < 1 \tag{9}$$

which gives

$$0 < K\cos(2\pi X_s) < 4. \tag{10}$$

Substituting Eq.(6) into Eq.(10), we obtain the stability condition as

$$|\,\Gamma - l\,| < \frac{K}{2\pi} < \{\frac{4}{\pi^2} + (\Gamma - l)^2\}^{\frac{1}{2}}. \tag{11}$$

In Fig.2), we illustrate the stability region defined by Eq.(11) for the values of $l = 0$ and $l = 1$. Thus, we can determine the positions of two islands observed for the values of $K = 3.3$ and $\Gamma = 0.5$ in Fig.1.c). With $l = 0$, Eq.(7) determines the position of the fixed point $X_0 = 0.2007$, while for the value of $l = 1$, Eq.(6) determines the position of the step-1 accelerator mode as $X_a = -0.2007$. It is interesting to note that neither the fixed point nor the step-1 accelerator mode exist in the triangle region $a\ b\ d$, thus the region appears to be completely chaotic, while the increase in the stochastic parameter K over the line $d\ b$ allows the onset of the step-1 accelerator mode.

Secondly, we can determine the critical value of $K(p/q)$ for the Poincaré-Birkhoff period-q bifurcation around the fixed point Eq.(7) from the tangent map Eq.(8) as

$$K(p/q) = 2\pi\{\Gamma^2 + \pi^{-2}(1 - \cos(2\pi p/q))^2\}^{\frac{1}{2}}, \tag{12}$$

or conversely, expressing $\Gamma(p/q)$ in terms of K

$$\Gamma(p/q) = \{(K/2\pi)^2 - \pi^{-2}(1-\cos(2\pi p/q))^2\}^{\frac{1}{2}}. \tag{13}$$

We remark that the values of $\Gamma(p/q)$ given by Eq.(13) determine the upper limit of the existence of the period-q Poincare-Birkhoff island for any given value of K.

Referring to Fig.1.b), for the value of $K = 2.1$, we estimate the value of Γ for the period-4 and period-5 island as

$$\Gamma(1/4) = 0.1010 \tag{14}$$

$$\Gamma(1/5) = 0.2516 \tag{15}$$

These numerical values are consistent with the observation in Fig.1.b). Turning to Fig.1.c), for the value of $K = 3.3$, we obtain the following values of Γ for the period-3, period-4 and period-5 islands,

$$\Gamma(1/3) = 0.2187, \tag{16}$$

$$\Gamma(1/4) = 0.4177, \tag{17}$$

$$\Gamma(1/5) = 0.4769. \tag{18}$$

The last three figures of Fig.1.c) are consistent with the results of Eqs.(17) and (18), while Eq.(16) is compatible with the observation of the period-3 squeezing at $\Gamma = 0.20$ in Fig.1.c).

Lastly, in order to analyze the period-3 squeezing in the Josephson map, following the analysis of the period-3 squeezing in the standard map[9], we derive the nonlinear quadratic map around the fixed point (X_f, P_f) defined by Eq.(7). Introducing the local variables (ξ_n, π_n) by the definition of

$$\begin{aligned} X_n &= X_f + \xi_n \\ P_n &= P_f + \pi_n, \end{aligned} \tag{19}$$

we obtain the nonlinear quadratic map

$$\begin{aligned} \xi_{n+1} &= \xi_n + \pi_{n+1} \\ \pi_{n+1} &= \pi_n + \alpha\xi_n + \beta\xi_n^2 \end{aligned} \tag{20}$$

where

$$\begin{aligned} \alpha &= K\cos(2\pi X_f) = (K^2 - 4\pi^2\Gamma^2)^{1/2}, \\ \beta &= -2\pi K\sin(2\pi X_f) = -4\pi^2\Gamma. \end{aligned} \tag{21}$$

One of the coordinate of the period-3 orbits (ξ_0, π_0) is determined to be

$$\begin{aligned} \xi_0^{(\pm)} &= \frac{1}{2\beta}\{\alpha - 2 \pm \sqrt{\alpha^2 - 8}\} \\ \pi_0 &= 0 \end{aligned} \tag{22}$$

where $\xi_0^{(+)}$ is the stable, while $\xi_0^{(-)}$ is the unstable period-3 orbit. Thus, the onset of the period-3 islands is determined from the condition $\alpha^2 > 8$ as

$$K > K_c \equiv (8 + 4\pi^2\Gamma^2)^{1/2}, \tag{23}$$

or

$$\Gamma_c \equiv (2\pi)^{-1}(K^2 - 8)^{1/2} > \Gamma. \tag{24}$$

For the value of $K = 3.3$, Eq.(24) gives rise to the upper limit of the existence of the period-3 island as $\Gamma_c = 0.2705$, which is consistent with the observation in Fig.1.c).

The squeezing takes place as $\xi_0^{(-)} \to 0$, which gives $\alpha = 3$, namely

$$K_s = (9 + 4\pi^2\Gamma^2)^{1/2}, \tag{25}$$

or

$$\Gamma_s = (2\pi)^{-1}(K^2 - 9)^{1/2}. \tag{26}$$

We notice that Eqs.(25) and (26) agree exactly with the Poincaré-Birkhoff period-3 bifurcation condition calculated by Eqs.(12) and (13). The value of Γ_s for $K = 3.3$ is 0.2187, as given by Eq.(16). We emphasize that the results of Eqs.(23) $\sim$ (26) are obtained from the nonlinear quadratic map, while Eqs.(12) and (13) are derived from the linearized tangent map.

4 Stochastic Diffusion in the Josephson Map

For given nonlinear dynamical systems, it is particularly interesting to examine their global statistical properties by investigating the stochastic diffusion processes. For the standard map[10], the numerical observation of the mean squared average spread of the orbits has been compared with the renormalized diffusion coefficient

$$\frac{D}{D_Q} = \frac{1 - 2J_1^2(K) - J_2^2(K) + 2J_3^2(K)}{(1 + J_2(K))^2} \tag{27}$$

with the abbreviation of $D_Q = (K/4\pi)^2$. The function $J_n(x)$ is the n-th Bessel function. The existence of various accelerator modes is responsible for the anomalous enhancement of the stochastic diffusion processes.

Since the bias Γ breaks the intrinsic symmetry of the standard map, it is extremely interesting subject to examine the stochastic diffusion associated with the Josephson map. The diffusion of the Josephson map is defined as

$$\begin{aligned} D &= \lim_{T\to\infty}\frac{1}{2T}\langle(P_T-P_0)^2\rangle \\ &= \lim_{T\to\infty}\frac{1}{2T}\sum_{j,k=1}^{T}\langle(\Delta P_j-\Gamma)(\Delta P_k-\Gamma)\rangle \end{aligned} \tag{28}$$

where the probabilistic variables ΔP_j is defined as

$$\Delta P_j = -A\sin(2\pi X_j)+\Gamma. \tag{29}$$

The bracket $\langle\ \rangle$ stands for the ensemble average over the initial distribution of the orbits. The correlation $C(k)$ is defined as

$$\begin{aligned} C(k) &= \langle(\Delta P_{T_0}-\Gamma)(\Delta P_{T_0+k}-\Gamma)\rangle \\ &= A^2\langle\sin(2\pi X_{T_0})\sin(2\pi X_{T_0+k})\rangle. \end{aligned} \tag{30}$$

With the help of the correlation $C(k)$, we can express the diffusion coefficient Eq.(28) as

$$D=\lim_{T\to\infty}\frac{1}{2}\sum_{k=1-T}^{T-1}\{1-\frac{k}{T}\}C(k)\simeq\frac{1}{2}C(0)+\sum_{k=1}^{\infty}C(k). \tag{31}$$

Defining the k-th order characteristic function χ_k by,

$$\chi_k(n_k,n_{k-1},\cdots,n_1,n_0)=\langle\exp 2\pi i\sum_{j=0}^{k}(n_jX_{T_0+j})\rangle \tag{32}$$

we can express the correlation $C(k)$ as

$$\begin{aligned} C(k) &= -\frac{1}{8\pi^2}K^2Re\left[\langle\exp 2\pi i(X_{T_0}+X_{T_0+k})\rangle-\langle\exp 2\pi i(X_{T_0}-X_{T_0+k})\rangle\right] \\ &= \frac{1}{8\pi^2}K^2Re\left[\chi_k(-1,0,\cdots,0,1)-\chi_k(1,0,\cdots,0,1)\right]. \end{aligned} \tag{33}$$

Collecting all of the principal terms, after the lengthy calculation, we obtain the renormalized diffusion coefficient

$$\begin{aligned} \frac{D}{D_Q} &= \frac{1}{(1-J_2^2(K))^2}\{1-2J_1^2(K)-J_2^2(K)+2J_3^2(K)\}\times \\ &\quad\times\{1-2J_2(K)\cos(2\pi\Gamma)+J_2^2(K)\}-4\frac{J_1^2(K)}{(1-J_2^2(K))^2}\sin^2(2\pi\Gamma) \end{aligned} \tag{34}$$

which is reduced to the diffusion coefficient of the standard map Eq.(27) for the limit of $\Gamma\to 0$.

In Fig.3) we show the diffusion coefficient Eq.(34) as the function of the stochastic parameter K for several values of the bias Γ. We observe that the bias Γ gives rise to nontrivial modification of the diffusion coefficient of the standard map Eq.(27). Thus, it becomes extremely interesting to compare the theoretical prediction with the numerical observation. Figs.4.a) and 4.b) illustrate the results of numerical observation for the values of $\Gamma = 0.25$ and $\Gamma = 0.50$, respectively. Here, we confirm that the accelerator modes give rise to the anomalous enhancement over the theoretical prediction of Eq.(34).

Much more detailed observation for the smaller values of the stochastic parameter $0 < K < 3$ for the same bias parameters are shown in Figs.5.a) and 5.b). For the standard map with $\Gamma = 0$, Greene[11] has identified the onset of the global stochasticity at the critical value of $K_c = 0.9716\cdots$. The present observations, however, suggest that the symmetry breaking by the bias Γ reduces the critical value of the global stochasticity by considerable amount. Basing on the results of Figs.5.a) and 5.b), we assign $K_c \approx 0.2$ for the value of $\Gamma = 0.25$, and $K_c \approx 0.5$ for the value of $\Gamma = 0.50$, respectively.

In order to get more explicit evidence, we explore the phase space structure of the Josephson map for the value of $\Gamma = 0.25$. In Fig.6), we show three portraits for the stochastic parameter $K = 0.10$, 0.20 and 0.30, respectively. For the value of $K = 0.10$, the phase space is separated into four regions, while for the value of $K = 0.20$ the whole phase space is connected, confirming the global stochasticity. We anticipate that the critical value is in the range of the $0.1 < K_c < 0.2$. We also notice that for the larger stochastic parameter $K = 0.3$, the period-4 and other coherent structure persist in the chaotic sea. We carry out the similar observation for the bias $\Gamma = 0.15$, for the stochastic parameter $0.1 < K < 1.0$. In Fig.7), we observe that the system is dominated by stochastic behavior even at the lowest value of $K = 0.1$. It is interesting to note that the increase in the stochastic parameter K enforces the occurrence of the periodic motion in the system.

To conclude the present section, we present here our preliminary results on the numerical observation of the diffusion coefficient at the smaller value of Γ in Fig.8). For the value of $\Gamma = 1/8 = 0.125$, we notice that the global diffusion sets in around $K_c \approx 0.1$, while for the much smaller values of $\Gamma = 1/40 = 0.025$, even at the small

value of $K \approx 0.1$, we observe considerable amount of the stochastic diffusion.

5 Concluding Remarks

In the present studies, we have shown that the external uniform bias imposed on the system described by the standard map gives rise to rich manifestation of the nonlinear behavior, with the sensitive dependence on the control parameters.

Our particular interests are focussed on the global stochastic behavior of the Josephson map. As discussed in the section 4, we observed a rather spectacular dependence of the diffusion coefficient on the small value of the bias Γ. Though our numerical observation is preliminary, it challenges us to undertake theoretical analysis on the effect of symmetry breaking in the nonlinear dynamical systems.

6 Acknowledgement

The present work has been supported by the JSPS program on Japan-FSU Scientists Collaboration. We are obliged to Professor K.Husimi for his constant encouragement. One of the authors (A.T.F) wishes to express his thanks to the kind hospitality to Yukawa Institute of Theoretical Physics and to Research Institute for Mathematical Sciences, Kyoto University. The authors wish to express their thanks to Professor T.Kamimura and the staff of the Computer Center at the National Institute for Fusion Science(NIFS). This work was supported by the Collaborating Program of NIFS.

References

[1] T.A.Fulton,R.C.Dynes and P.W.Anderson, Proc.IEEE **61** (1973),28

[2] D.W.McLaughlin and A.C.Scott, Phys. Rev. A **18** (1978), 1652

[3] Yu.S.Gal'pern and A.T.Filippov, JETP Lett. **35** (1982), 580

[4] A.T.Filippov and Yu.S.Gal'pern, Solid State Commun. **48** (1983), 665

[5] Yu.S.Gal'pern and A.T.Filippov, Sov.Phys. JETP **59** (1984), 894

[6] A.T.Filippov, Yu.S.Gal'pern, T.L.Boyadjiev and I.V.Puzynin, Phys. Lett. A, **120** (1987), 47

[7] A.N.Vystavkin, Yu.F.Drachevsky, V.P.Koshelets and I.L.Serpuchenko, Fiz. Niz. Temp. **14** (1988), 646. see also Proc. Int. Superconductor Electronics Conf. ISEC-89, Tokyo (1989)

[8] A.T.Filippov and Yu.S.Gal'pern, Phys. Lett. A **172** (1993),471

[9] Y.H.Ichikawa, T.Kamimura, T.Hatori and S.Y.Kim, Prog. Theoret. Phys. Suppl. **98** (1989) 1

[10] Y.H.Ichikawa, T.Kamimura and T.Hatori, Physica D **29** (1987), 247

[11] J.M.Green, J. Math. Phys. **20** (1979), 1183

Captions of Figures

Fig.1

Phase space portrait of the Josephson map for the stochastic parameters ; a) $K = 1.3$, b) $K = 2.1$ and c) $K = 3.3$. The number attached to each frame stands for the value the bias Γ.

Fig.2

The curve **a b c** represents the upper limit of the stochastic parameter K for the fixed point with $l = 0$, while the curve **f c** stands for the upper limit of the stochastic parameter A for the step-1 accelerator mode.

Fig.3

The renormalized diffusion coefficient Eq.(34) for the value of $\Gamma = 0, 0.1, 0.25, 0.35$ and 0.5.

Fig.4

Numerical observation of the stochastic diffusion ; a) for $\Gamma = 0.25$ and b) for $\Gamma = 0.5$. Observed diffusion deviates from the theoretical prediction in the hatched region where the accelerator modes exist.

Fig.5

Numerical observation of the stochastic diffusion in the region of the small stochastic parameter $K < 3.0$; a) for $\Gamma = 0.25$, b) for $\Gamma = 0.50$

Fig.6

Phase space portrait of the Josephson map for the value of $\Gamma = 0.25$; a) for the stochastic parameter $K = 0.10$, b) for $K = 0.20$ and c) for $K = 0.30$, respectively.

Fig.7

Phase space portrait of the Josephson map for the value of $\Gamma = 0.15$; a) for $K = 0.10$ b) for $K = 0.20$, c) for $K = 0.30$ d) for $K = 0.80$ and e) for $K = 1.00$.

Fig.8

Numerical observation of the stochastic diffusion for the values of $\Gamma = 1/8 = 0.125$, $\Gamma = 3/40 = 0.075$ and $\Gamma = 1/40 = 0.025$.

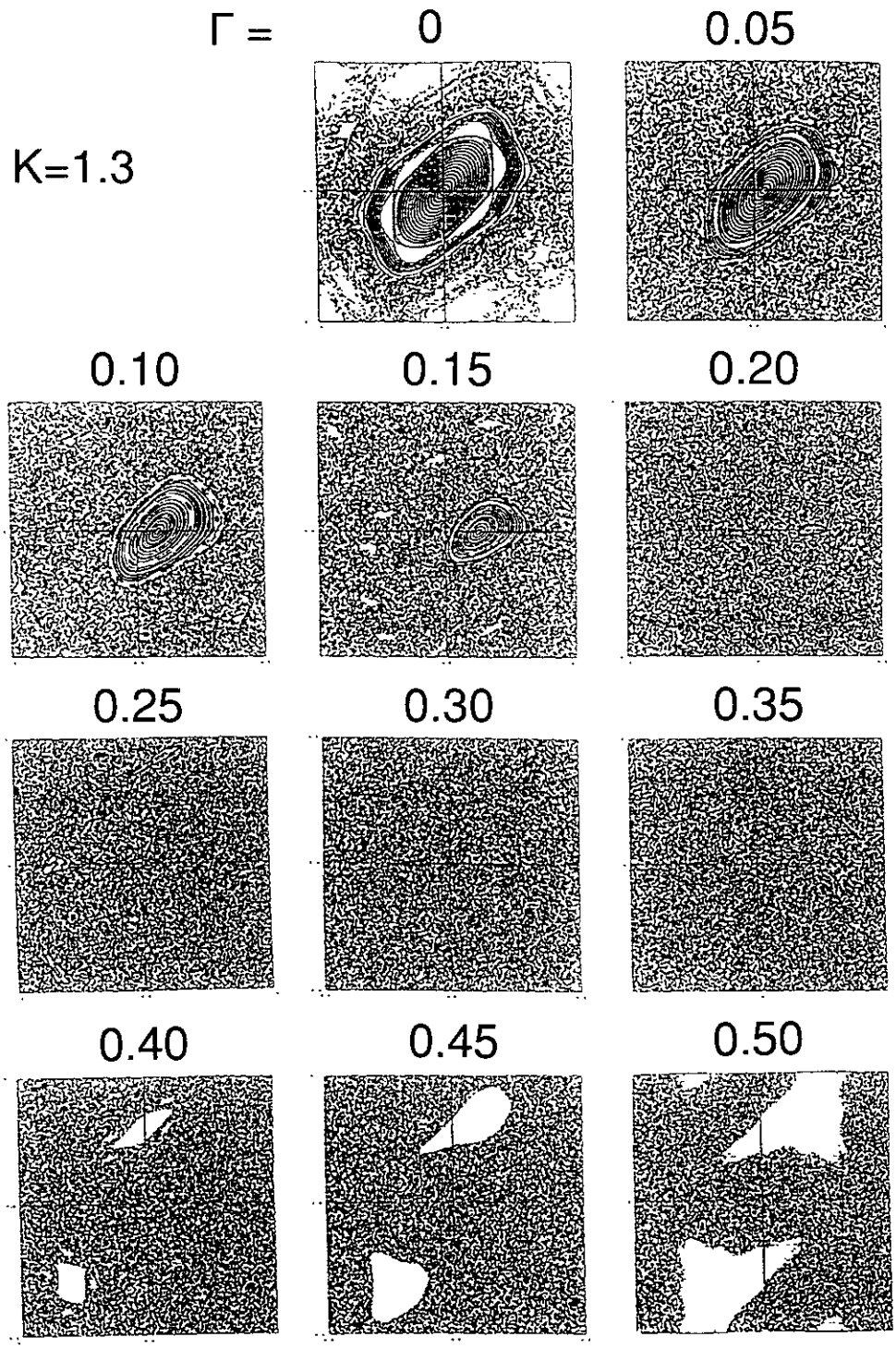

Fig. 1 a)

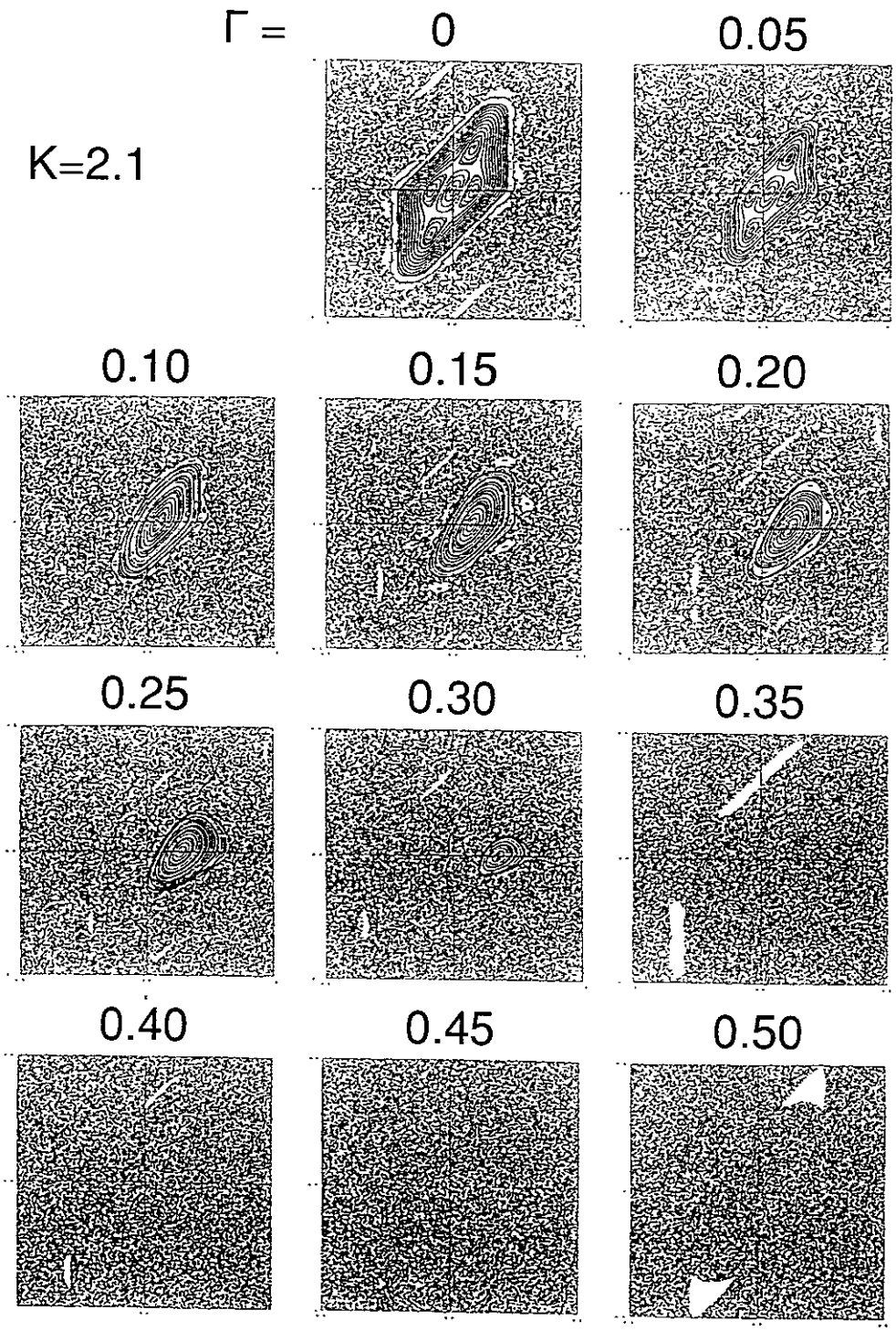

Fig. 1 b)

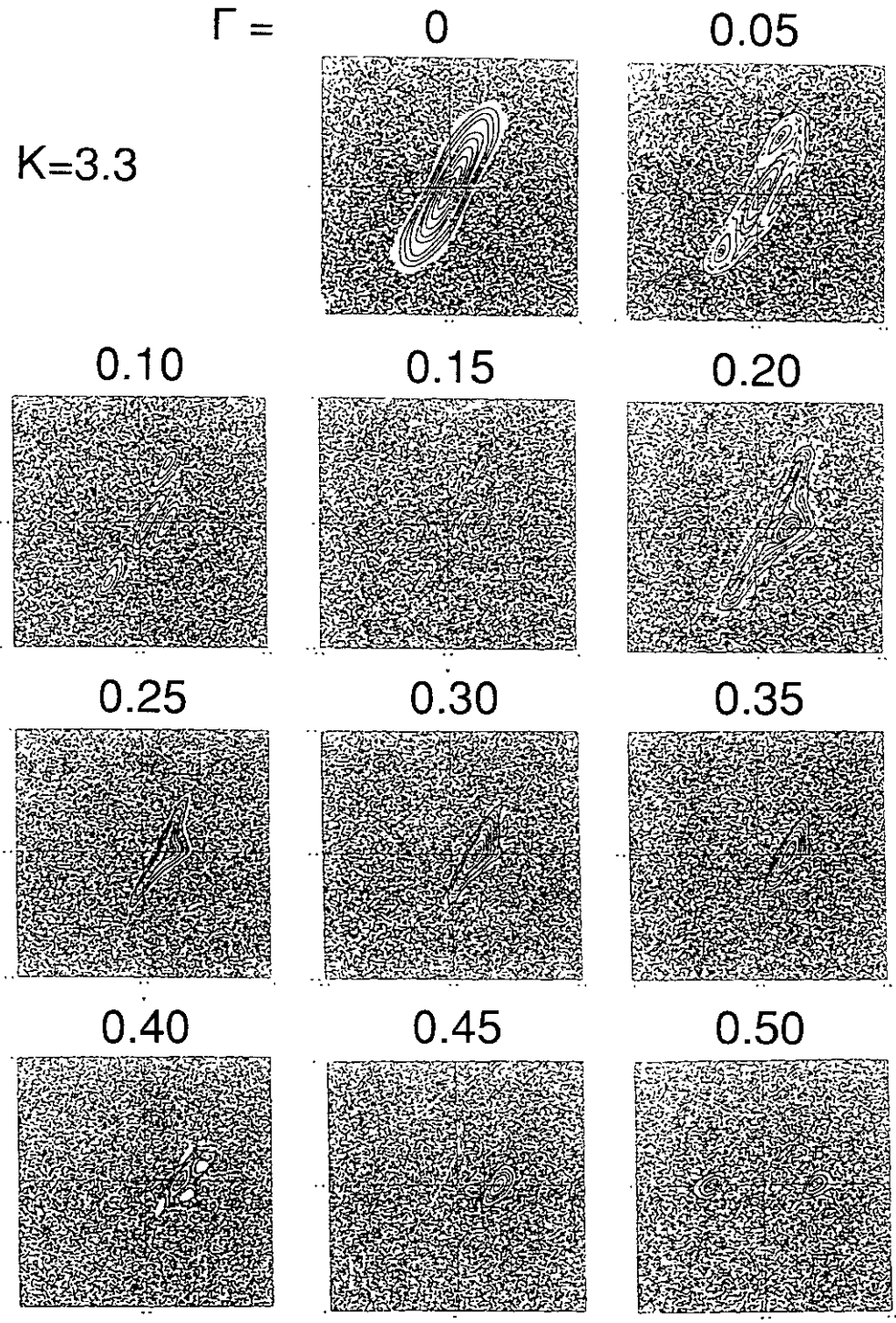

Fig. 1 c)

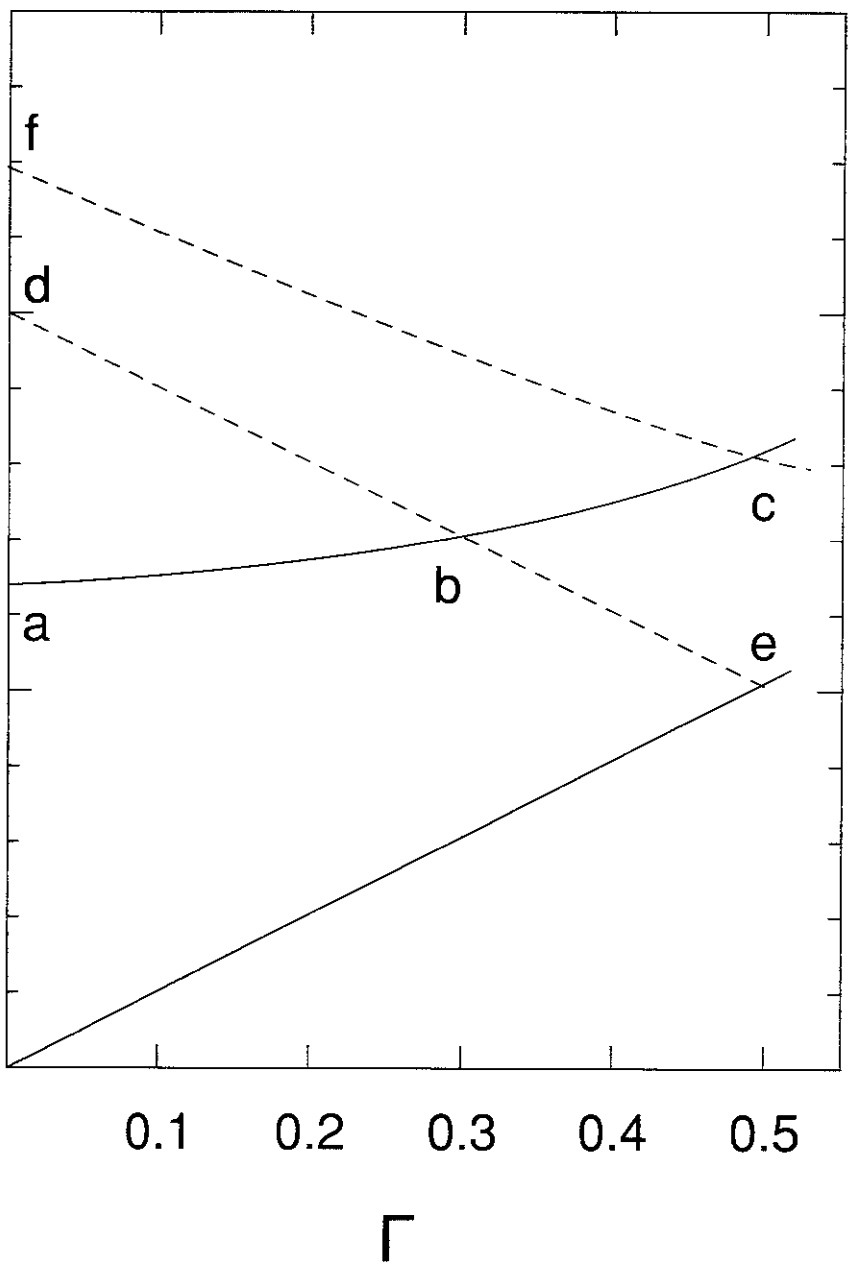

Fig. 2

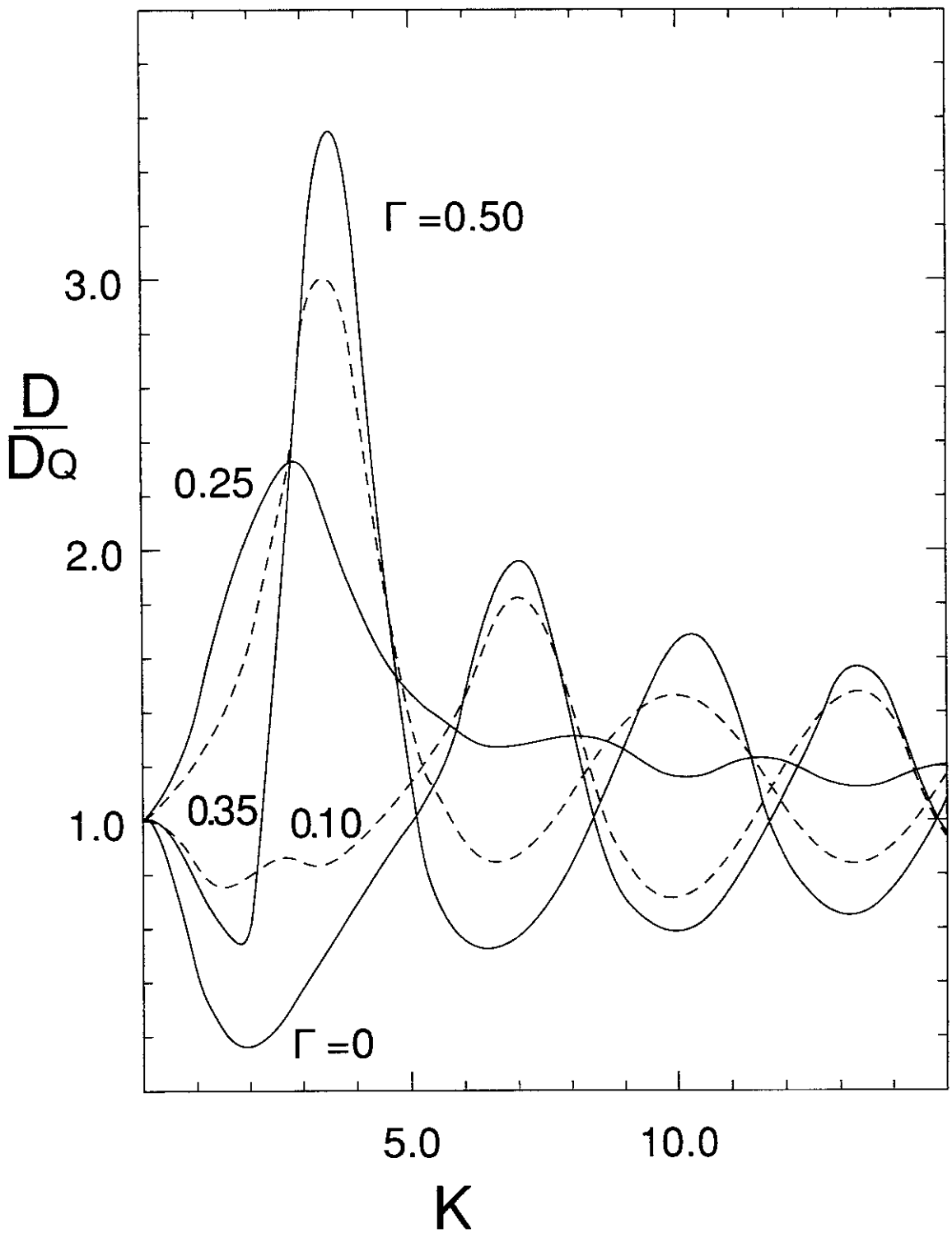

Fig. 3

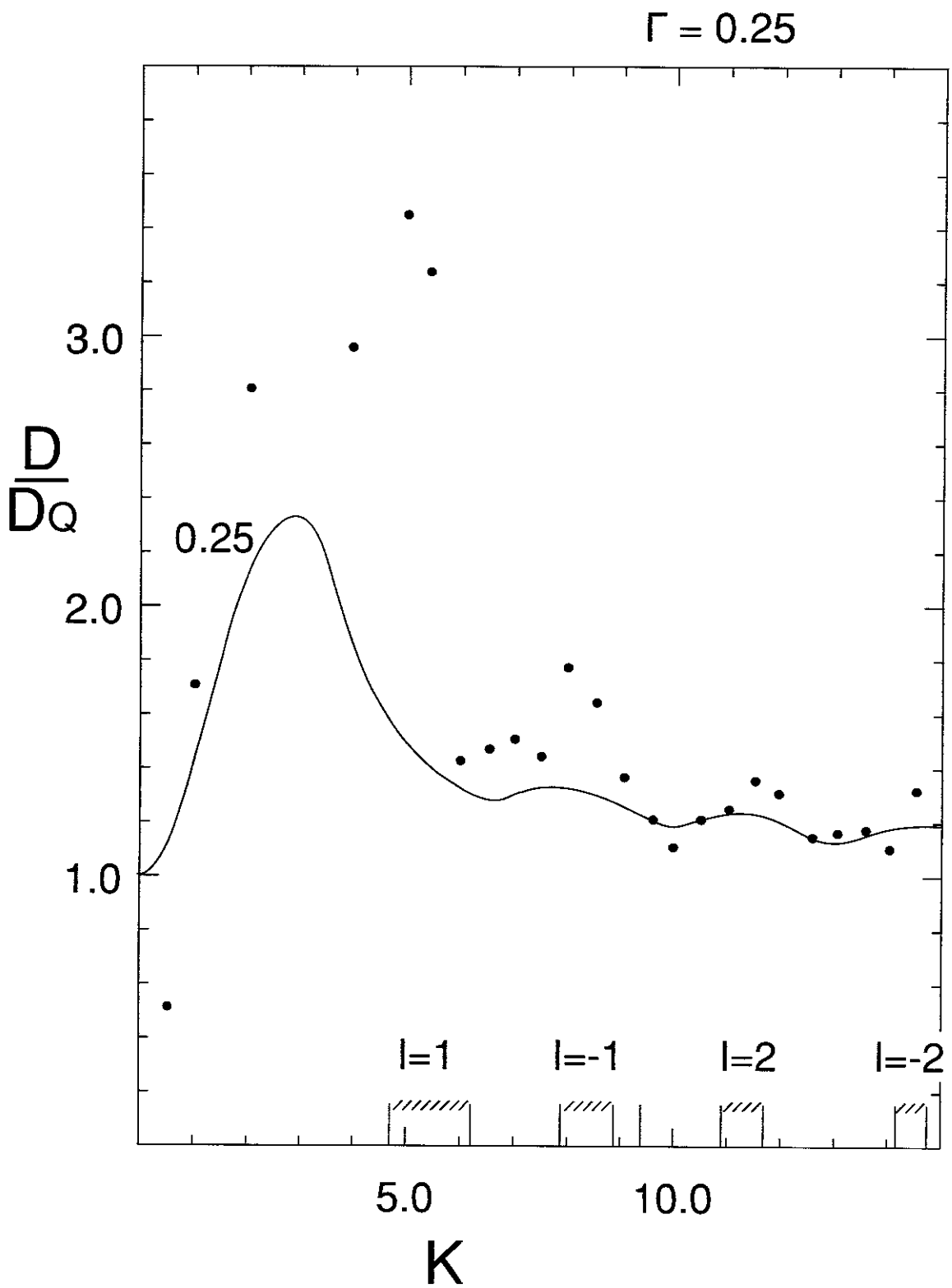

Fig. 4 a)

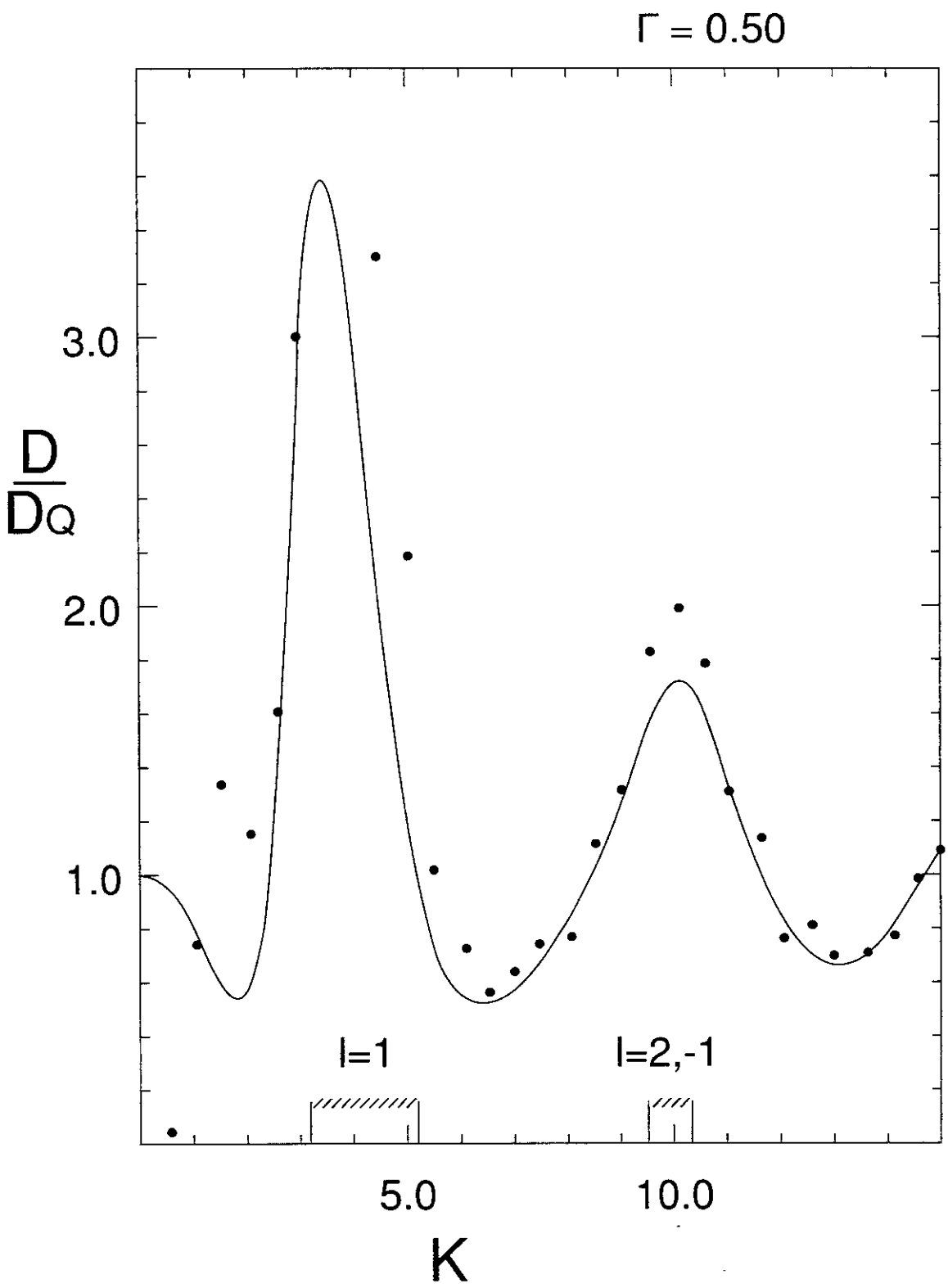

Fig. 4 b)

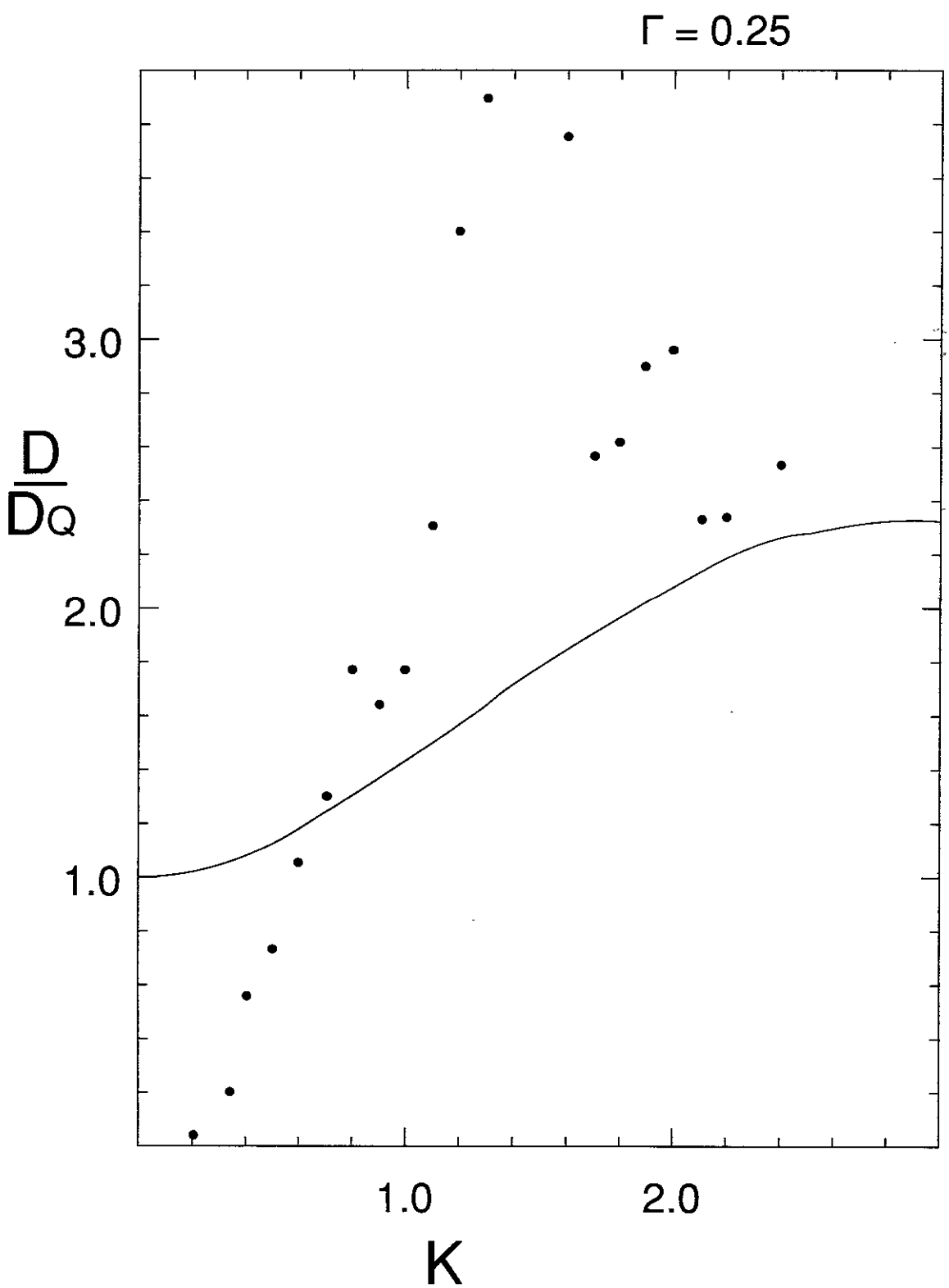

Fig. 5 a)

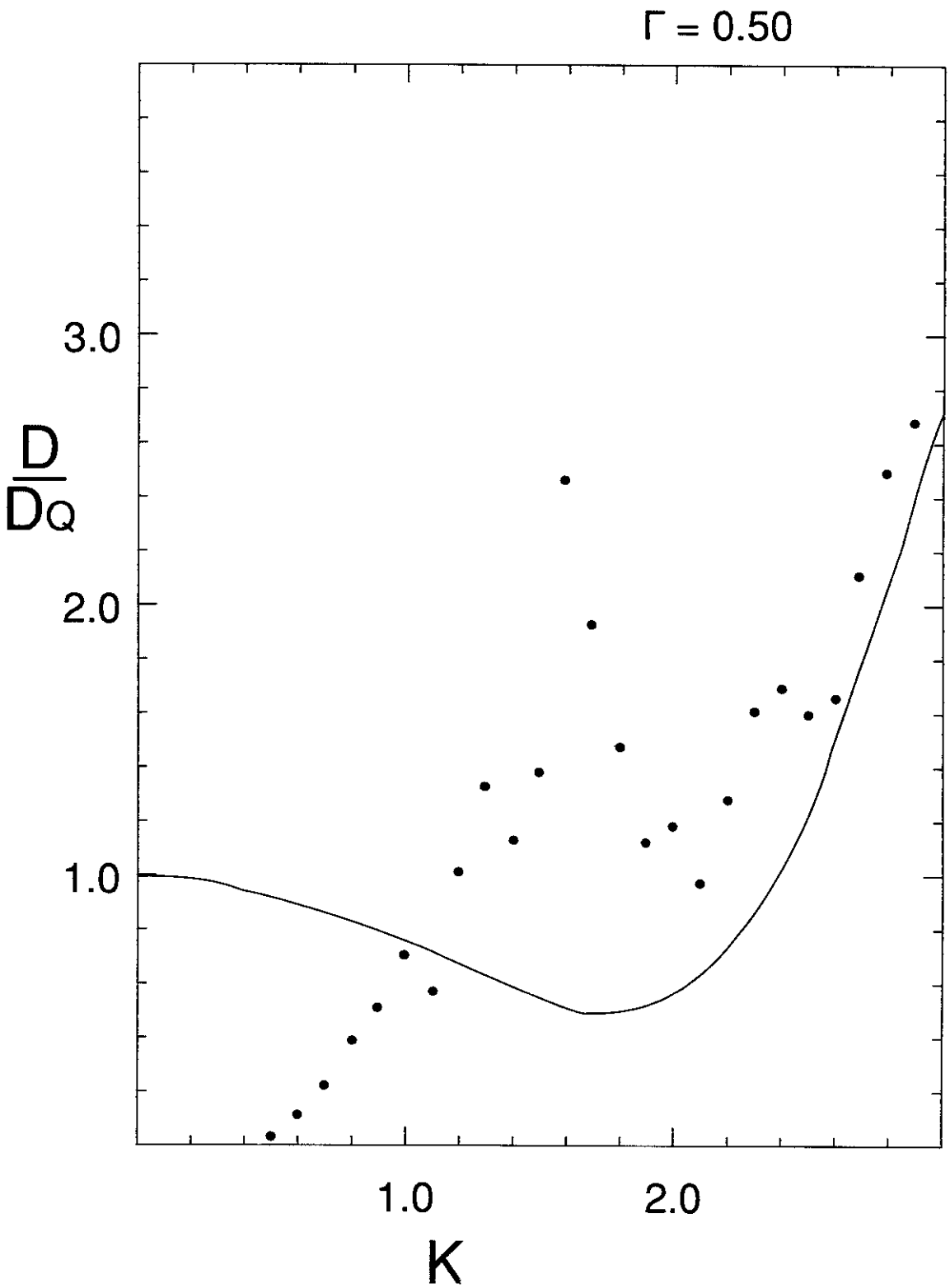

Fig. 5 b)

a)

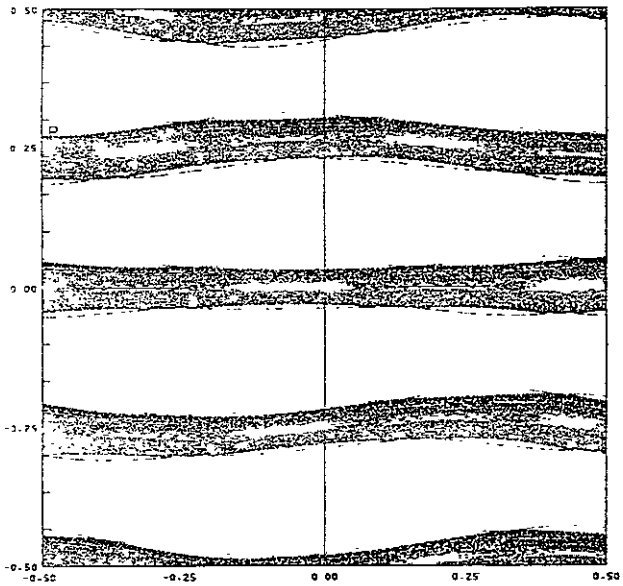

Γ =0.25

K=0.1

b)

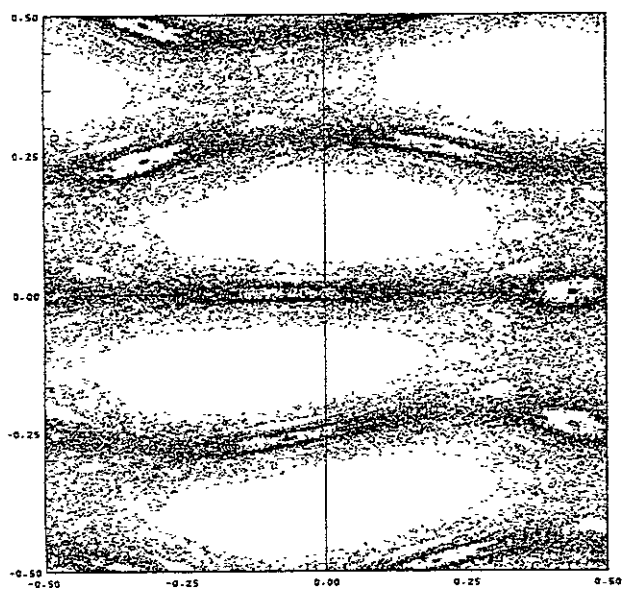

K=0.2

c)

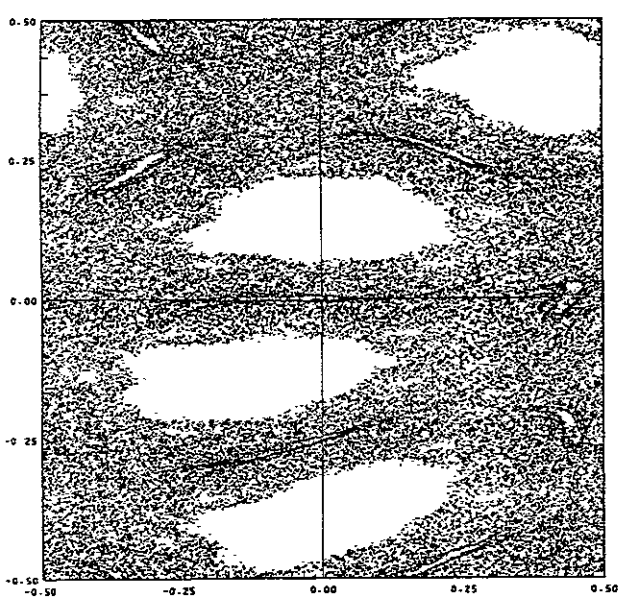

K=0.3

Fig. 6

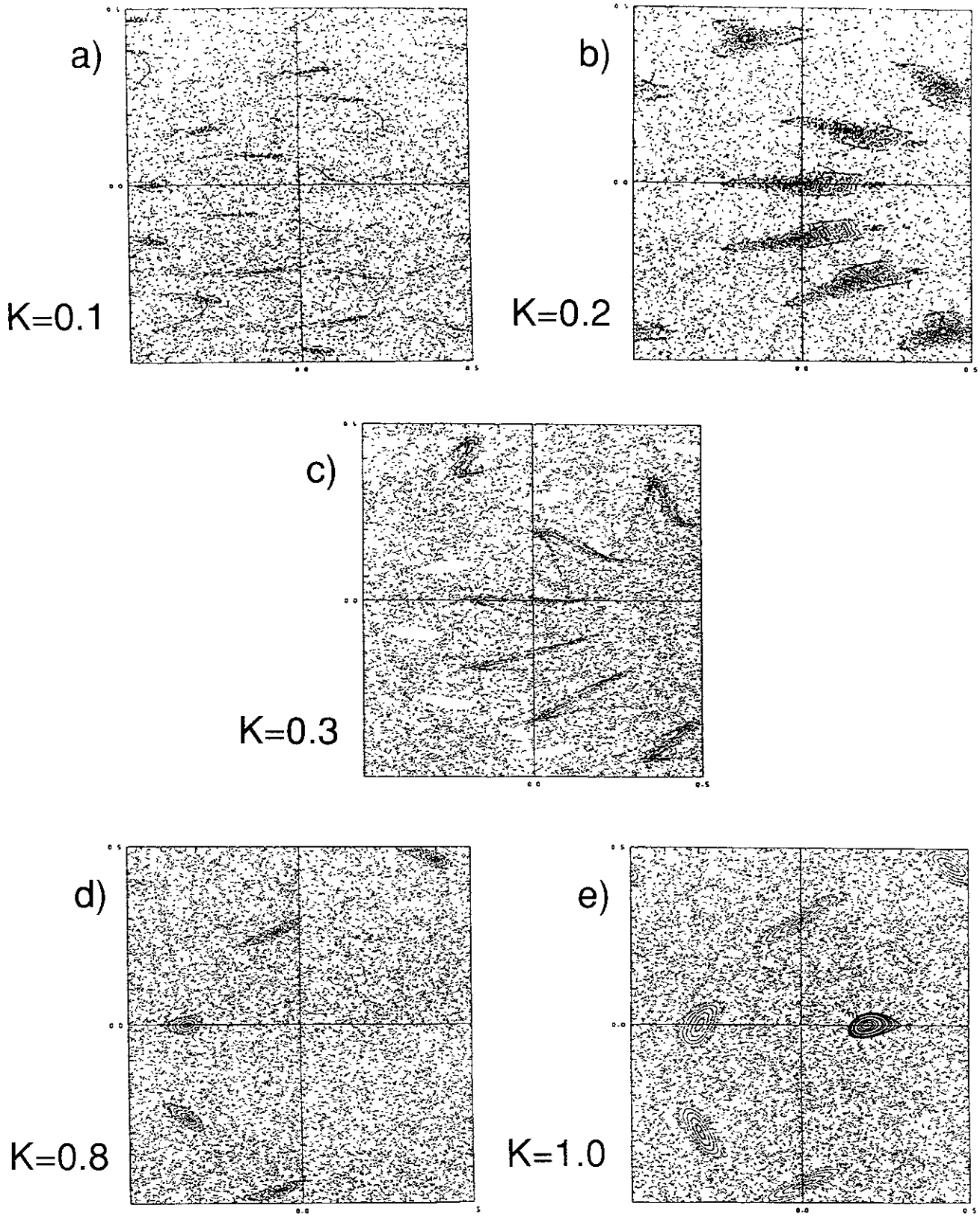

Fig. 7

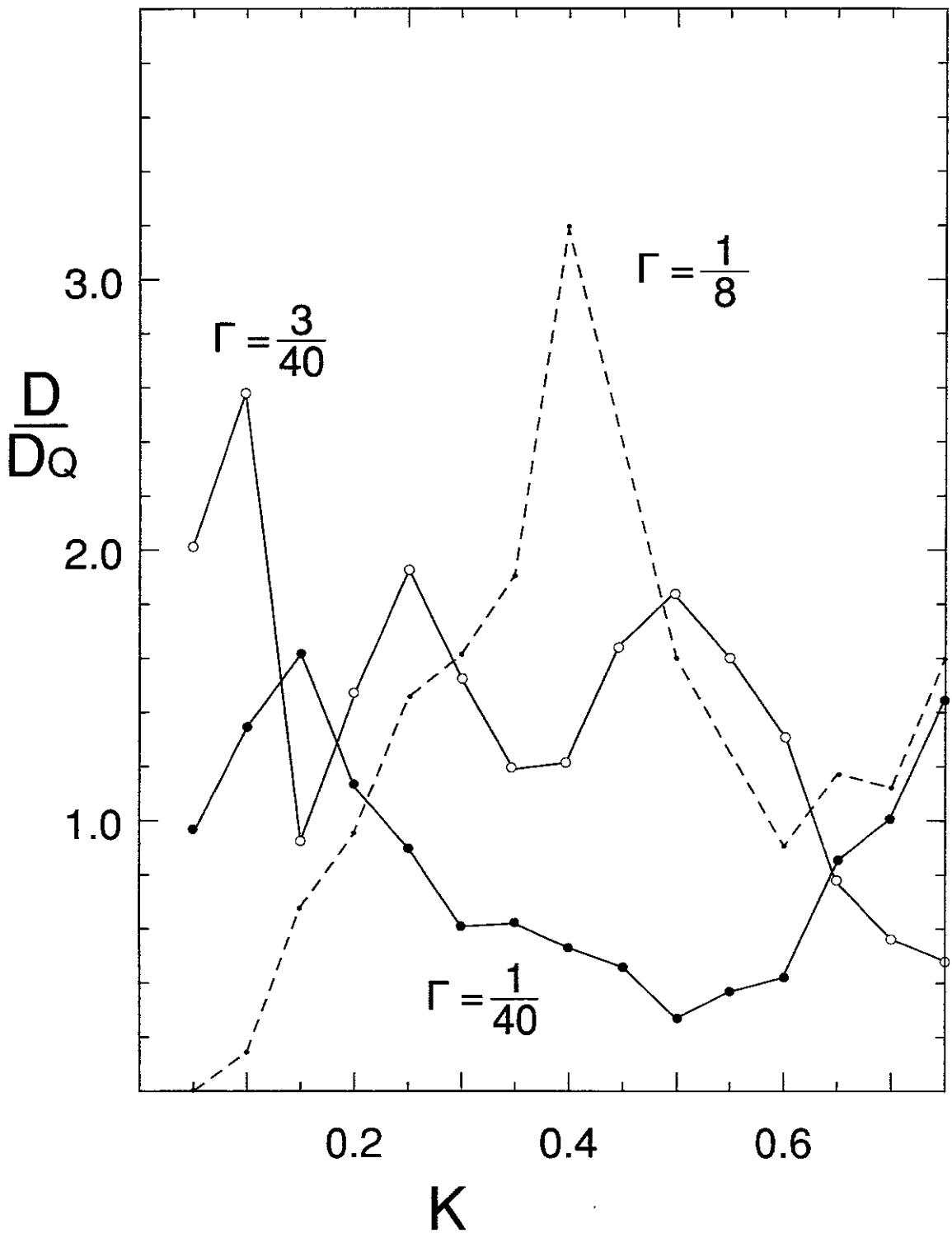

Fig. 8

Recent Issues of NIFS Series

NIFS-365 K. Itoh, S.-I. Itoh, A. Fukuyama and M. Yagi,
On the Minimum Circulating Power of Steady State Tokamaks; July 1995

NIFS-366 K. Itoh and Sanae-I. Itoh,
The Role of Electric Field in Confinement; July 1995

NIFS-367 F. Xiao and T. Yabe,
A Rational Function Based Scheme for Solving Advection Equation; July 1995

NIFS-368 Y. Takeiri, O. Kaneko, Y. Oka, K. Tsumori, E. Asano, R. Akiyama, T. Kawamoto and T. Kuroda,
Multi-Beamlet Focusing of Intense Negative Ion Beams by Aperture Displacement Technique; Aug. 1995

NIFS-369 A. Ando, Y. Takeiri, O. Kaneko, Y. Oka, K. Tsumori, E. Asano, T. Kawamoto, R. Akiyama and T. Kuroda,
Experiments of an Intense H- Ion Beam Acceleration; Aug. 1995

NIFS-370 M. Sasao, A. Taniike, I. Nomura, M. Wada, H. Yamaoka and M. Sato,
Development of Diagnostic Beams for Alpha Particle Measurement on ITER; Aug. 1995

NIFS-371 S. Yamaguchi, J. Yamamoto and O. Motojima;
A New Cable -in conduit Conductor Magnet with Insulated Strands; Sep. 1995

NIFS-372 H. Miura,
Enstrophy Generation in a Shock-Dominated Turbulence; Sep. 1995

NIFS-373 M. Natsir, A. Sagara, K. Tsuzuki, B. Tsuchiya, Y. Hasegawa, O. Motojima,
Control of Discharge Conditions to Reduce Hydrogen Content in Low Z Films Produced with DC Glow; Sep. 1995

NIFS-374 K. Tsuzuki, M. Natsir, N. Inoue, A. Sagara, N. Noda, O. Motojima, T. Mochizuki, I. Fujita, T. Hino and T. Yamashina,
Behavior of Hydrogen Atoms in Boron Films during H_2 and He Glow Discharge and Thermal Desorption; Sep. 1995

NIFS-375 U. Stroth, M. Murakami, R.A. Dory, H. Yamada, S. Okamura, F. Sano and T. Obiki,
Energy Confinement Scaling from the International Stellarator Database; Sep. 1995

NIFS-376 S. Bazdenkov, T. Sato, K. Watanabe and The Complexity Simulation Group,

Multi-Scale Semi-Ideal Magnetohydrodynamics of a Tokamak Plasma; Sep. 1995

NIFS-377 J. Uramoto,
Extraction of Negative Pionlike Particles from a H2 or D2 Gas Discharge Plasma in Magnetic Field; Sep. 1995

NIFS-378 K. Akaishi,
Theoretical Consideration for the Outgassing Characteristics of an Unbaked Vacuum System; Oct. 1995

NIFS-379 H. Shimazu, S. Machida and M. Tanaka,
Macro-Particle Simulation of Collisionless Parallel Shocks; Oct. 1995

NIFS-380 N. Kondo and Y. Kondoh,
Eigenfunction Spectrum Analysis for Self-organization in Dissipative Solitons; Oct. 1995

NIFS-381 Y. Kondoh, M. Yoshizawa, A. Nakano and T. Yabe,
Self-organization of Two-dimensional Incompressible Viscous Flow in a Friction-free Box; Oct. 1995

NIFS-382 Y.N. Nejoh and H. Sanuki,
The Effects of the Beam and Ion Temperatures on Ion-Acoustic Waves in an Electron Beam-Plasma System; Oct. 1995

NIFS-383 K. Ichiguchi, O. Motojima, K. Yamazaki, N. Nakajima and M. Okamoto
Flexibility of LHD Configuration with Multi-Layer Helical Coils; Nov. 1995

NIFS-384 D. Biskamp, E. Schwarz and J.F. Drake,
Two-dimensional Electron Magnetohydrodynamic Turbulence; Nov. 1995

NIFS-385 H. Kitabata, T. Hayashi, T. Sato and Complexity Simulation Group,
Impulsive Nature in Collisional Driven Reconnection; Nov. 1995

NIFS-386 Y. Katoh, T. Muroga, A. Kohyama, R.E. Stoller, C. Namba and O. Motojima,
Rate Theory Modeling of Defect Evolution under Cascade Damage Conditions:The Influence of Vacancy-type Cascade Remnants and Application to the Defect Production Chracterization by Microstructural Analysis; Nov. 1995

NIFS-387 K. Araki, S. Yanase and J. Mizushima,
Symmetry Breaking by Differential Rotation and Saddle-node Bifurcation of the Thermal Convection in a Spherical Shell; Dec. 1995

NIFS-388 V.D. Pustovitov,
Control of Pfirsch-Schlüter Current by External Poloidal Magnetic Field

in Conventional Stellarators: Dec. 1995

NIFS-389 K. Akaishi,
On the Outgassing Rate Versus Time Characteristics in the Pump-down of an Unbaked Vacuum System; Dec. 1995

NIFS-390 K.N. Sato, S. Murakami, N. Nakajima, K. Itoh,
Possibility of Simulation Experiments for Fast Particle Physics in Large Helical Device (LHD); Dec. 1995

NIFS-391 W.X.Wang, M. Okamoto, N. Nakajima, S. Murakami and N. Ohyabu,
A Monte Carlo Simulation Model for the Steady-State Plasma in the Scrape-off Layer; Dec. 1995

NIFS-392 Shao-ping Zhu, R. Horiuchi, T. Sato and The Complexity Simulation Group,
Self-organization Process of a Magnetohydrodynamic Plasma in the Presence of Thermal Conduction; Dec. 1995

NIFS-393 M. Ozaki, T. Sato, R. Horiuchi and the Complexity Simulation Group
Electromagnetic Instability and Anomalous Resistivity in a Magnetic Neutral Sheet; Dec. 1995

NIFS-394 K. Itoh, S.-I Itoh, M. Yagi and A. Fukuyama,
Subcritical Excitation of Plasma Turbulence; Jan. 1996

NIFS-395 H. Sugama and M. Okamoto, W. Horton and M. Wakatani,
Transport Processes and Entropy Production in Toroidal Plasmas with Gyrokinetic Eletromagnetic Turbulence; Jan. 1996

NIFS-396 T. Kato, T. Fujiwara and Y. Hanaoka,
X-ray Spectral Analysis of Yohkoh BCS Data on Sep. 6 1992 Flares - Blue Shift Component and Ion Abundances -; Feb. 1996

NIFS-397 H. Kuramoto, N. Hiraki, S. Moriyama, K. Toi, K. Sato, K. Narihara, A. Ejiri, T. Seki and JIPP T-IIU Group,
Measurement of the Poloidal Magnetic Field Profile with High Time Resolution Zeeman Polarimeter in the JIPP T-IIU Tokamak; Feb. 1996

NIFS-398 J.F. Wang, T. Amano, Y. Ogawa, N. Inoue,
Simulation of Burning Plasma Dynamics in ITER; Feb. 1996

NIFS-399 K. Itoh, S-I. Itoh, A. Fukuyama and M. Yagi,
Theory of Self-Sustained Turbulence in Confined Plasmas; Feb. 1996

NIFS-400 J. Uramoto,
A Detection Method of Negative Pionlike Particles from a H2 Gas Descharge Plasma; Feb. 1996

NIFS-401 K.Ida, J.Xu, K.N.Sato, H.Sakakita and JIPP TII-U group,

Fast Charge Exchange Spectroscopy Using a Fabry-Perot Spectrometer in the JIPP TII-U Tokamak; Feb. 1996

NIFS-402 T. Amano,
Passive Shut-Down of ITER Plasma by Be Evaporation; Feb. 1996

NIFS-403 K. Orito,
A New Variable Transformation Technique for the Nonlinear Drift Vortex; Feb. 1996

NIFS-404 T. Oike, K. Kitachi, S. Ohdachi, K. Toi, S. Sakakibara, S. Morita, T. Morisaki, H. Suzuki, S. Okamura, K. Matsuoka and CHS group;
Measurement of Magnetic Field Fluctuations near Plasma Edge with Movable Magnetic Probe Array in the CHS Heliotron/Torsatron; Mar. 1996

NIFS-405 S.K. Guharay, K. Tsumori, M. Hamabe, Y. Takeiri, O. Kaneko, T. Kuroda,
Simple Emittance Measurement of H- Beams from a Large Plasma Source; Mar. 1996

NIFS-406 M. Tanaka and D. Biskamp,
Symmetry-Breaking due to Parallel Electron Motion and Resultant Scaling in Collisionless Magnetic Reconnection; Mar. 1996

NIFS-407 K. Kitachi, T. Oike, S. Ohdachi, K. Toi, R. Akiyama, A. Ejiri, Y. Hamada, H.Kuramoto, K. Narihara, T. Seki and JIPP T-IIU Group,
Measurement of Magnetic Field Fluctuations within Last Closed Flux Surface with Movable Magnetic Probe Array in the JIPP T-IIU Tokamak; Mar. 1996

NIFS-408 K. Hirose, S. Saito and Yoshi.H. Ichikawa
Structure of Period-2 Step-1 Accelerator Island in Area Preserving Maps; Mar. 1996

NIFS-409 G.Y.Yu, M. Okamoto, H. Sanuki, T. Amano,
Effect of Plasma Inertia on Vertical Displacement Instability in Tokamaks; Mar. 1996

NIFS-410 T. Yamagishi,
Solution of Initial Value Problem of Gyro-Kinetic Equation; Mar. 1996

NIFS-411 K. Ida and N. Nakajima,
Comparison of Parallel Viscosity with Neoclassical Theory; Apr. 1996

NIFS-412 T. Ohkawa and H. Ohkawa,
Cuspher, A Combined Confinement System; Apr. 1996

NIFS-413 Y. Nomura, Y.H. Ichikawa and A.T. Filippov,
Stochasticity in the Josephson Map; Apr. 1996